

Microbial activity records in Marinoan Snowball Earth postglacial transition layers connecting diamictite with cap carbonate (Otavi Group, NW-Namibia)

Ildikó GYOLLAJ¹⁾²⁾, Márta POLGÁRI²⁾³⁾⁴⁾, Krisztián FINTOR⁴⁾, Elemér PÁL-MOLNÁR⁴⁾, Friedrich POPP⁵⁾ & Christian KOEBERL¹⁾⁶⁾

¹⁾ Department of Lithospheric Research, University of Vienna, Althanstrasse 14, A-1090 Vienna, Austria;

²⁾ Research Center for Astronomy and Geosciences, Geobiomineralization and Astrobiological Research Group, Institute for Geology and

³⁾ Geochemistry, Hungarian Academy of Sciences, 1112 Budapest, Budaörsi str. 45, Hungary;

⁴⁾ Eszterházy Károly University, Dept. of Physical Geography and Geoinformatics, Leányka str. 6, 3300 Eger, Hungary;

⁵⁾ Szeged University, Department of Mineralogy, Geochemistry and Petrology, Egyetem str. 2-6, 6702 Szeged, Hungary;

⁶⁾ Department of Geodynamics and Sedimentology, University of Vienna, Althanstrasse 14, A-1090 Vienna, Austria;

⁶⁾ Natural History Museum, Vienna, A-1010 Burggring 7, Vienna, Austria;

^{*)} Corresponding author, rodokrozit@gmail.com

KEYWORDS Snowball Earth; deglaciation; microbial mats; iron-oxidizing bacteria; biodegradation; cap carbonate; Otavi Group; NW-Namibia

Abstract

This study concerns the microbial mat formation in postglacial layers of the Marinoan Snowball Earth glaciation. A high resolution investigation was carried out on the transition layers of Ghaub to Maieberg Formation (start of Keilberg Member) of the Otavi Group in NW-Namibia (Neoproterozoic). Macroscopic characterization, optical rock microscopy, XRD mineralogy, Raman spectroscopy investigations were done and geochemical (major and trace element content) as well as carbonate carbon isotopic data were collected. Three types of microbial contributions were determined: (1) primary, synsedimentary Fe-rich biomats; (2) secondary biomats from biodegradation of Fe-bearing minerals (pyrite, chlorite); and (3) pseudo-secondary structures coating on clasts. These microbial mats of iron-oxidizing bacteria consumed iron from different sources, such as hydrothermal solutions or iron-bearing minerals. On the basis of the morphology of Fe-biomats, and the mineralogical and geochemical signatures, we suggest that the Marinoan postglacial transition layers (Ghaub-Maieberg boundary) formed under neutral, suboxic conditions in brackish water at the studied locality.

1. Introduction

The Cryogenian Period (~720–635 Ma) comprises an important interval of the Neoproterozoic characterized by dramatic tectonic, climatic, and biological changes, including global glaciations. The "Snowball Earth" hypothesis suggests that the Earth was more or less covered by ice sheets during the Neoproterozoic glaciation periods (Hoffman et al., 1998b). The hypothesis of Neoproterozoic Snowball Earth glaciations, as summarized by Fairchild and Kennedy (2007), was based on different hypothetical models: Hard Snowball Earth (Hoffman et al., 1998a), Slushball Earth (Harland, 1964), and, high-tilt Earth (Williams, 2000). At least two glacial events occurred during the Neoproterozoic, the older Sturtian (750 Ma) and the younger Marinoan event. According to Re-Os isotope dating, the Marinoan glaciation occurred around 635 Ma ago (Rooney et al., 2015). Glaciogenic sediments were preserved worldwide, including in northern Namibia.

Breakup of the supercontinent Rodinia began around 750 Ma (Eyles and Janaszczak, 2004) with the formation of rift basins on the margins, interpreted to influence significantly Earth's climate. Significant increase of continental margins and intensified magmatic activity enhanced subaerial silicate weathering and drew down atmospheric CO₂ levels, triggering the global glaciation of the Cryogenian (Hoffman and Schrag, 2002).

Concurrently with these global tectonic and climatic events, stepwise oxygenation resulted in metallogenesis and production of large deposits of banded iron formations (BIF) (Le Heron et al., 2013). Besides ore formations, these glaciogenic sediments also represent hydrocarbon source rocks (Bechstädt et al., 2009; Gaschnig et al., 2014).

Signs of microbial activity in the form of *laminated microbial carbonate layers*, *tube-like columnar stromatolites* are globally widespread in the sediments of Neoproterozoic Sturtian and Marinoan deglaciation also in Otavi Group, NW Namibia, and discussed in detail by several authors (Bechstädt et al., 2009; Le Ber et al., 2013; Le Heron et al., 2013 and references therein). Likewise, Fraiser and Corsetti (2003) discovered structures that formed by microbial (calcified bacterial clumps) and diagenetic processes. Pruss et al. (2010) reported microbial facies (including thinly laminated, slowly lithified mats rolling up into roll-up structures) in the Sturtian Rasthof Formation, Otavi Group, northern Namibia, considered as the signature of potential biogenic provenance in cap carbonate sediments formed below the storm base.

The tidal cap carbonates included stromatolite-like microbial structures at other localities, which contained carbonates, phosphate and various clay minerals, such as smectite, glau-

conite, palygorskite, which were deposited under suboxic conditions (e.g., in Oman, Mettreux et al., 2015). The fluctuation of Mg and Sr isotopic ratios in Marinoan cap carbonates signified oscillation of postglacial oceans, which were influenced by

seafloor volcanism and weathering (e.g., Tarim Craton, NW-China, Wen et al., 2015). The Marinoan postglacial shallow-water carbonates originated from microbial carbonate factories, which extended into a deep supratidal facies at the top

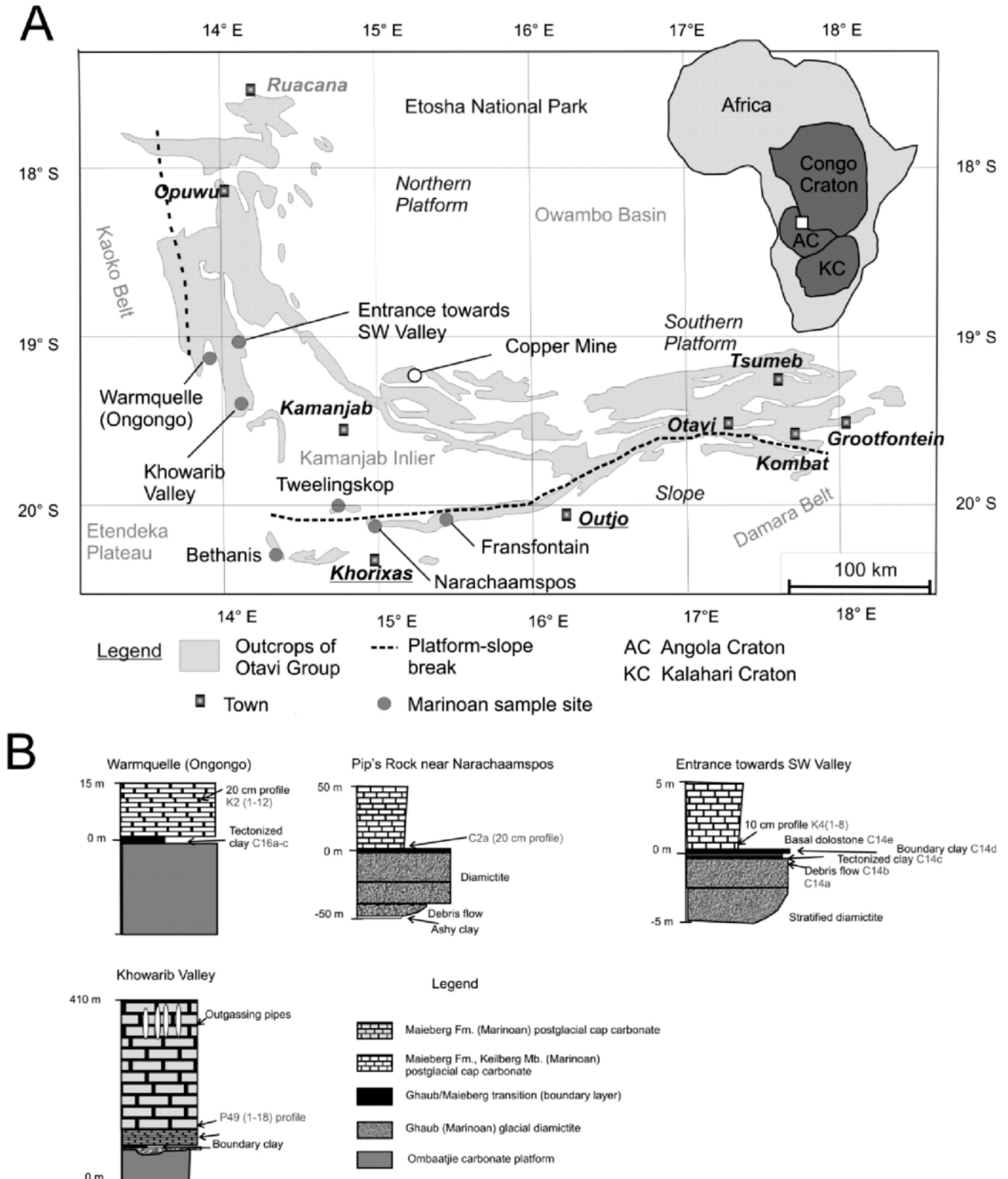


Figure 1: Sampling sites of Marinoan postglacial layers with map of outcrop of Otavi Group (A), and profiles (B) (modified after Hoffman (2002)). 1A: the platform-slope facies boundary is marked by a black dashed line. 1B: Stratigraphic position of profiles (Warmquelle, Entrance towards SW Valley, Narachaamspos) showing biogenic samples (K2, K4, C2a, C14a). Khorwarib Valley (P49-1), Fransfontain (C1), and Bethanis (C7) are shown in Fig. 1 A.

of the stratigraphic column in the Central African Niari Basin (Mickala et al., 2015).

The microbially mediated formations also contain Fe-rich sediments, globally widespread Cryogenian ironstones (e.g., the Chuos Formation in Namibia), which have been attributed to post-Snowball Earth ice meltback, and local hydrothermal input as a consequence of the breakdown of Rodinia (Le Heron et al., 2013, and references therein). For the source of Fe anoxic deeper-water conditions and iron content of Neoproterozoic postglacial oceans can be addressed, although the tidal areas were oxic (van Smeerdijk Hood and Wallace, 2015). For the Fe enrichment the analogy of recent acidophile biomats was used, as photosynthetic bacteria fix CO₂ and Fe intracellularly (Le Heron et al., 2013).

Recently *Fe-rich thin-bedded layers, mineralized microbially produced sedimentary structures (MMPSS)* from shallow water environments were reported from the postglacial transition layers (Chuos Fm./Rasthof Fm.) of the Namibian Otavi Group as an example of a series of ancient Fe-rich biomats formed at the sediment/water interface under neutrophylic and sub-oxic conditions (Gyollai et al., 2015).

Oolitic carbonate sandstones from the basal layer of the Rasthof Fm., was also studied (Gyollai et al., 2014a). The distinct hydrocarbon content was considered to originate from bacterial (probably cyanobacteria) communities that existed in shallow water environments of the ancient Otavi platform. Smectite surrounding the ooid grains was most probably derived from diagenesis and/or weathering of microbial films (Gyollai et al., 2014a).

This study provides information on microbially mediated Fe-rich sediments related to the deglaciation process in the aftermath of the younger Cryogenian Period, Otavi Group, NW-Namibia. The goal of research is to derive paleoenvironmental implications during the sedimentation and secondary processes of the Marinoan postglacial layers (Keilberg Member at the base of Maieberg Formation overlying Ghaub glaciogenic sediments, Tsumeb Subgroup, Otavi Group), for distinguishing the primary and/or secondary origin of Fe-rich biomats according to nutrient sources.

2. Geological background

Our investigations concern the transition from the Ghaub Formation to the Maieberg Formation of the Otavi Group, Tsumeb Subgroup, in NW-Namibia. The studied layers are considered to represent the sedimentary conditions during the immediate transition interval from the glacial environment of the Marinoan ice age towards the subsequent climatic warm interval. These postglacial transition layers span the uppermost/lowermost portions of the Ghaub/Maieberg formations (Keilberg Member) in the Western Otavi platform area.

Here, the Ghaub Formation is only partially preserved within structural depressions of inner platform areas (Hoffman and Prave, 1996), suggesting that the Otavi bank fell dry at low sea water level during glacial periods, thus being one of the source areas for appreciable diamictite accumulations in

slope facies areas bordering on the platform edges (Fig. 1A, Gyollai et al., 2014ab, 2015). The Ghaub glacial lithofacies are composed almost exclusively of carbonate debris with numerous clasts of various size, composed of dolomite and rarely limestone, all apparently derived from the underlying Omabaatjie Formation (Hoffman and Halverson, 2008; Bechstädt et al., 2009).

Stratigraphic evidence points to a single sea-level advance and retreat cycle during the Ghaub glaciation; grounded ice existed at the maximum rise leaving characteristic “ice rafted”, sedimentary features (Domack and Hoffman, 2003, 2011).

On top of the diamictites there is a cap carbonate succession represented by limestones and dolomites at the base, and overlying dark colored dolomitic shale, belonging to the Maieberg Formation (Bechstädt et al., 2009).

This formation, subdivided into three members, constitutes an up to 400-m-thick pile of cyclic deposits that originated on a warm periodic platform carbonate facies environment following the Ghaub glacial period (Hedberg, 1979; SACS, 1980). The basal Keilberg Member is a “cap dolostone” associated with the sea-level rise during the Ghaub deglaciation (Hoffmann and Prave, 1996; Hoffman and Schrag, 2000; Kennedy et al., 2001). Its characteristic feature is a uniform, 10-15 m thick, pale-colored marker bed which is internally laminated on a mm-scale and shows characteristic small-scale, low angle cross-stratification. Lamination is caused by higher clay and silt content. Pyrite and hematite are common (Bechstädt et al., 2009 and references therein). Pyrite (mm scale) occurs as disseminated euhedral grains and in veins and lenses. This suggests syndepositional deposition of pyrite in anoxic conditions, but diagenetic formation is also proposed. The Maieberg cap carbonate dolostone shows paleogeographical and stratigraphical variability in the Otavi Mountains from inner platform to slope environments.

Unusual sedimentary structures featuring vertical “tube-like” appearance are visible, starting about one meter above the base, at our sampling sites. These tubes may have been generated as a result of CO₂ oversaturation (Le Hir et al., 2008; Bechstädt et al., 2009; Le Ber et al., 2013; Le Heron et al., 2013) and methane outgassing from clathrates (Kennedy et al., 2008). According to another hypothesis, the tubes may have formed in close connection with the growth of stromatolites (Hoffman and Halverson, 2008).

More details on the geological background of the studied area are given by Gyollai et al. (2014a,b, 2015).

3. Samples and methods

3.1 Samples

Samples were collected from layers closest to/above the boundary between the uppermost Ghaub glacial diamictite and the basal post-glacial cap dolomite (Keilberg Mb./Maieberg Fm.). A total of fifty-two samples from different paleogeographic regions of the Otavi Group in northern Namibia were analyzed, all containing microbial structures (Fig. 1AB

and Table 1). They originated from distal slope facies deposits abutting against the Otavi platform at outcrops near Fransfontain (sample C1(abc); 20°11'59.06"S; 15° 0'58.68"E), near Narachaamspos (sample C2a; 20°11'27.68"S; 14°51'4.42"E) and Bethanis (sample C7; 20°24'21.95"S; 14°20'35.06"E) (Fig. 1B and Fig. 2AB). Outcrops, representing inner Otavi platform facies conditions are located within the Khowarib Fold Belt near Ongongo, Warmquelle (sample K2; 19° 8'35.77"S; 13°51'15.40"E; Fig. 1B), at the head of a valley extending from Entrance (near Devede village) towards the SW (samples K4 and C14a; 19°11'18.40"S; 13°56'13.39"E; Fig. 1B and Fig. 2CDE) and at the hillside of the Khowarib Valley (sample P49-1; 19°18'24.52"S; 13°59'25.57"E; Fig. 1B).

Besides those samples (sub-samples), which contain signs of microbial mediation, the following datasets were also investigated by detailed geochemical analyses to characterize their formation conditions: Narachaamspos (samples C2bc, C3_1,2, C17 abc); Bethanis (sample C6); Tweelingskop (samples C4, C5); Entrance towards SW Valley (samples C14bcde, C15abcd); Khowarib Valley (sample C15e); Warmquelle (samples C16abc) (for localities see Fig. 1A).

3.2 Methods

The lithology of our samples was described by macroscopic observation and optical microscopy (Table 1). The textural analysis of the specific microbial structures were obtained by optical microscopy (Research Centre for Geology and Geochemistry, Hungarian Academy of Sci-

Thin sections	Stratigraphic setting with locality	Lithology	Microbial structures
K4-3*	Maieberg Fm. Keilberg Mb – profile Entrance towards SW Valley inner platform facies	kinked detrital layer interbedding in dolomite tectonic overprint (sausage/boudinage structure-like detritus layers, sigma clasts: shearing tectonics clay lenses: alteration of original biomats	filamentous iron bacteria- (colonial coccolid cells, sheath-enclosed colonial unicells and spheroidal unicells) K4-1 well preserved, K4-2 weathered, progressive weathering of biogenic structures to clay minerals in Profile K4
K4-2	Maieberg Fm. Keilberg Mb – profile Entrance towards SW Valley inner platform facies	detrital layer: wavy lamination (locally broken)	
K4-1	Maieberg Fm. Keilberg Mb – profile Entrance towards SW Valley inner platform facies	micritic dolomite with detrital layers cement: calcite, quartz under detrital layer carbonate shows flow structure, above the detrital layer unstratified carbonate diagenetic overprint	
C14a	Ghaub Fm. Entrance towards SW Valley inner platform facies	top of red diamictite platform facies debris flow with large carbonate blocks and with mica among the blocks cement: micrite iron-oxide	filamentous iron bacteria at the boundary of clasts
K2-2	Warmquelle inner platform facies	dolomite with fine-grained well- stratified structure fluidization structures (flame and ball structures) diagenetic overprint	1. primary structures: filamentous iron bacteria (coccolid spheroidal colonial cells) 2. secondary structures along fractures (bioweathering)
K2-1	Warmquelle inner platform facies		weathered (smectite-bearing) microbial mat in iron rich layer and diagenetic quartz (filamentous cyanobacteria iron bacteria (coccolid colonial cells)
P49-1	Khowarib Valley inner platform facies		bioweathering crust
C1c	Ghaub/Maieberg Fm. (boundary) Fransfontain slope facies	fine grainstone interbedding of terrigenous strata (silt, quartz arenite) ripple-lamination (quartz strata), angular cross lamination (iron-oxide and clay strata)	cyanobacteria (numerous) filamentous iron bacteria (colonial coccolid cells and spheroidal unicells)
C1b	Ghaub/Maieberg Fm. (boundary) Fransfontain slope facies	fine-grained grainstone with extraclasts	filamentous iron bacteria (coccolid unicells)
C2a-7	Maieberg Fm. Keilberg Mb Narachaamspos slope facies	carbonate ball and flame structure – fluidization pyrite-quartz-clay sigma clasts	weathered, putative filamentous iron bacteria (colonial coccolid cells, sheath- enclosed colonial unicells and spheroidal unicells)
C2a-6	Maieberg Fm. Keilberg Mb Narachaamspos slope facies	flow structure with diagenetic quartz and carbonate rich layer sigma clast of pyrite and quartz	moderate weathering, coccolid-forming biomat of putative iron bacteria filamentous cyanobacteria
C2a-5	Maieberg Fm. Keilberg Mb Narachaamspos slope facies	carbonate with pyrite-quartz sigma clasts – metamorphic overprint iron-bearing wavy lamination and carbonate layers	weathered filamentous iron bacteria- (colonial coccolid cells, sheath-enclosed colonial unicells and spheroidal unicells) (main occurrence in pyrite - quartz lens, and in surrounding carbonate)
C2a-4	Maieberg Fm. Keilberg Mb Narachaamspos slope facies		black and red filamentous iron bacteria (colonial coccolid cells, sheath-enclosed colonial unicells and spheroidal unicells) in pyrite lens (low weathering rate)
C2a-3	Ghaub/Maieberg Fm. Narachaamspos slope facies	micritic carbonate, thin detrital layer interbedding	
C2a-2	Ghaub Fm. (top)	coarse detrital layers in carbonate micritic-coarse carbonate rhythmic bedding	
C2a-1	Narachaamspos slope facies		
C7	Bethanis slope facies	carbonate green-schist facies, metamorphosed sedimentary structures: fine plane lamination of carbonate layers, climbing lamination in iron oxide containing detrital layer cement: sericite, micrite	cyanobacteria filamentous iron bacteria (colonial coccolid and spheroidal cells)

Table 1: Lithology of Marinoan samples containing microbial structures

number of subsamples: profile K4–8, profile K2–11, profile C2a–17, * for locality see Fig. 1.

ences, Budapest), and by a Thermo Scientific DXR confocal edge filter-based microRaman spectrometer with 10 mW, 532 nm diode-pumped solid state laser excitation system, and thermoelectrically cooled charged coupled device array detector (Department of Mineralogy, Geochemistry and Petrology, University of Szeged) for the identification of mineral phases.

X-ray diffraction data (XRD) were collected by a Phillips diffractometer (PW 3710, goniometer PW-1820), CuK α radiation (45 kV, 35 mA), step size of 0.02 degrees, and counting time of 1 s per step (Department of Geodynamics and Sedimentology, University of Vienna). Minerals were identified using the Joint Committee on Powder Diffraction Standards (1980) database.

The contents of Fe and trace elements were determined by instrumental neutron activation analyses (INAA) at the Department of Lithospheric Research, University of Vienna. Contents

of major elements and some trace elements (Cu, Ni, Co, Sc, Cr, V) were measured on bulk rock samples by X-ray fluorescence (XRF) spectrometry, using a Philips PW 2400 sequential X-ray spectrometer equipped with a Rh-excitation source (Department of Lithospheric Research, University of Vienna).

Carbon isotopic compositions of bulk samples were determined at the Department of Lithospheric Research, University of Vienna, using a Carlo Erba Elemental Analyzer coupled to a Micromass Optima stable isotope ratio mass spectrometer. From each sample, about 300–600 mg powder was weighed into tin capsules. Each powder sample was analyzed at least three times with a precision between 0.04 ‰ and 0.31 ‰. The $\delta^{13}\text{C}$ values were calculated relative to the V-PDB isotopic composition. As laboratory standards, replicate analyses of a graphite (USGS-24, Coplen et al., 2006) and of a carbonate (NBS-18; Verkouteren and Klindinst, 2004) were used; accuracy was better than 0.7 ‰ for USGS-24 and better than

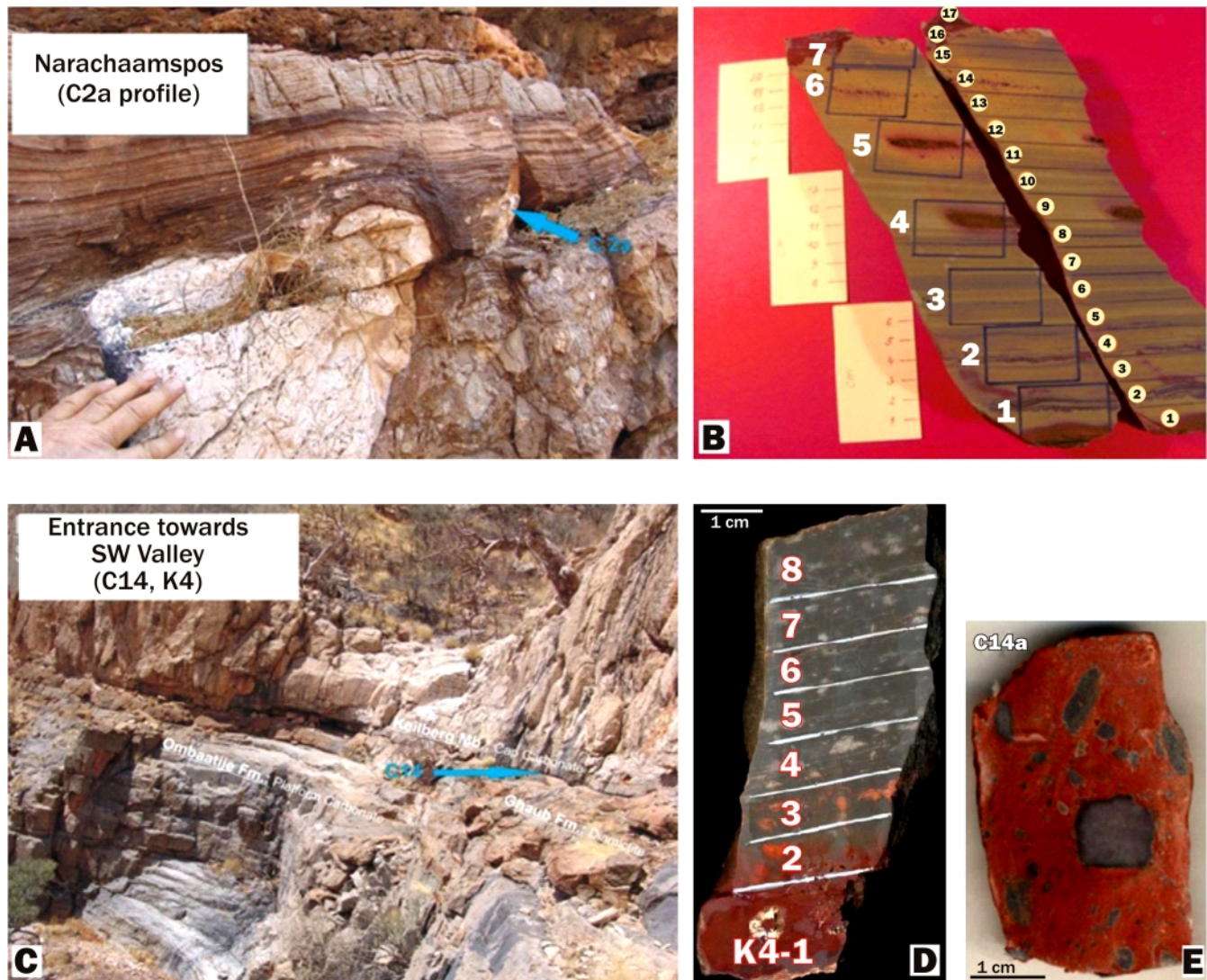


Figure 2: Photos of outcrops and sections of selected samples at Narachaamspos (distal slope facies, C2a), and Entrance towards SW Valley (inner platform facies, K4, C14a). The Narachaamspos outcrop is shown in 2A, its lithological profile is shown in 2B (C2a profile – pyrite-bearing detritus interval in carbonate with well visible lamination, scale is the same as on D). The outcrop from Entrance towards SW Valley is shown in 2C and its lithological profile is shown on 2D (K4 profile – calcite lens beds in dark micrite) (modified after Gyollai et al., 2014b, Fig. 5), and diamictite sample on 2E (C14a – quartz pebble clasts in reddish micrite).

0.2 ‰ for NBS-18. For details of the method, including accuracy and precision, see Maruoka et al. (2003, 2007).

4. Results

4.1 Petrography of microbial structures

The microscopically analyzed samples enclosing in-situ microbial structures came primarily from the distal slope facies deposits and from outcrops representing inner Otavi platform facies deposits. In general, the samples are characterized by gray-white-reddish brown color and micritic texture, but samples at the border zone with subjacent diamictites contain layers with clastic particles (samples C2a and C14a). The thickness of the layers containing microbial structures varies from millimeters to a few centimeters. Within the studied Marinoan postglacial layers we detected three distinct types of microbial mats with respect to their microfacies and interpreted formation conditions: (i) Type 1 - syn-sedimentary mats, trapping sediment particles (profile K4, sample C1); (ii) Type 2 - secondary mats, resulting from bioweathering of iron-bearing minerals (pyrite, chlorite) (profiles C2a and K2, samples C7, P49-1); and (iii) Type 3 - biofilm coatings on clast surfaces, formed directly after their deposition in the bedrock (C14a).

4.1.1 Type 1 microbial structures: Primary, synsedimentary biomat structures

Thin, wavy laminated, reddish-brown Fe-rich structures within ~1-2 cm thick layers composed of micritic carbonate matrix form characteristic successions; these layers include filamentous Fe-rich structures resembling to *Gallionella/Mariprofundus*-like biosignatures (Chan et al., 2011; Konhauser, 2012), organic mate-

rial and clay minerals (smectite) (Fig. 3AB). Tiny, cubic shaped opaque minerals might be pyrite, which display loading structures incising the sedimentary lamination (Fig. 3AB). The loading structures were caused by settling of cubic pyrite crystals, which cause disturbance in lamination because of its

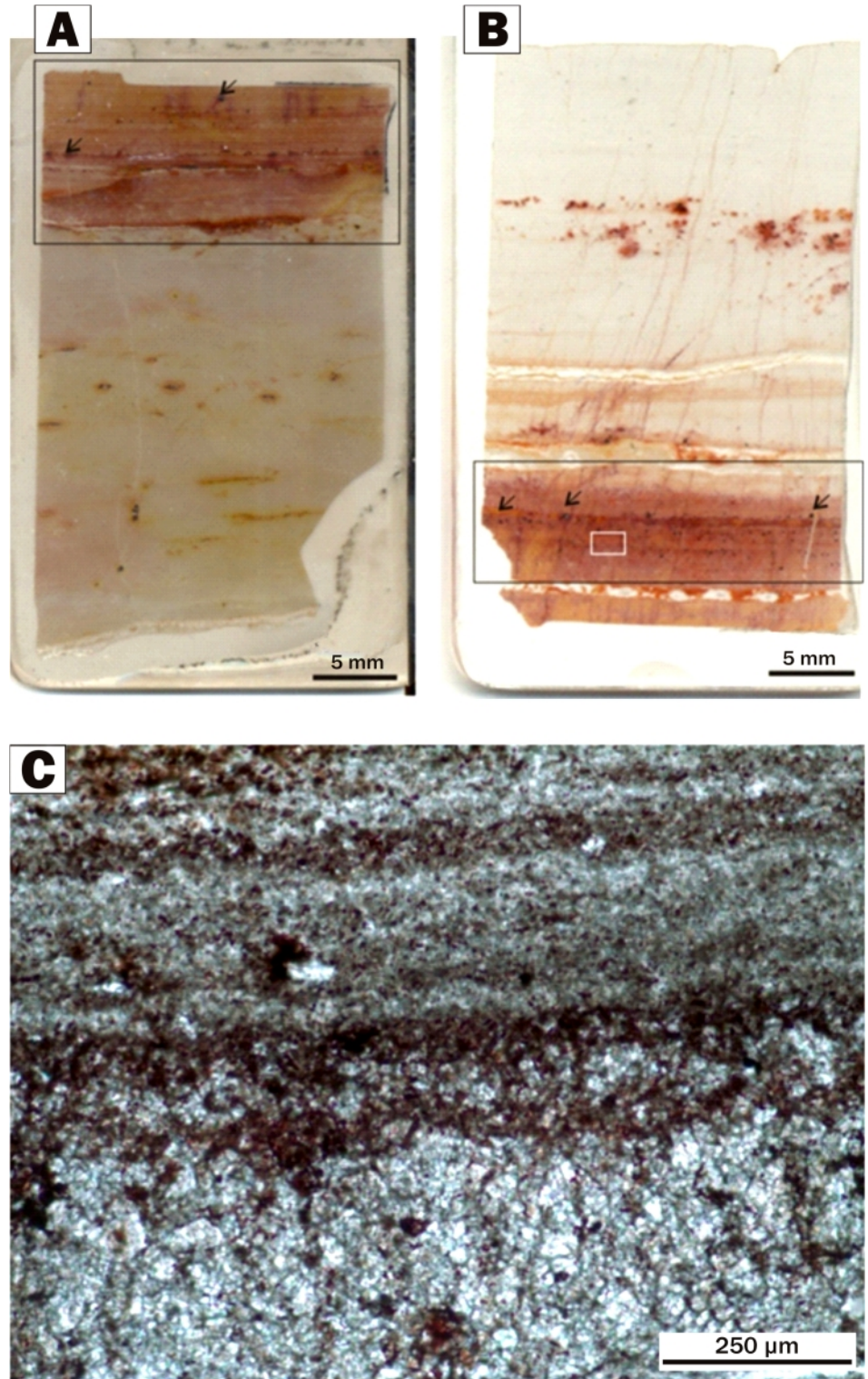
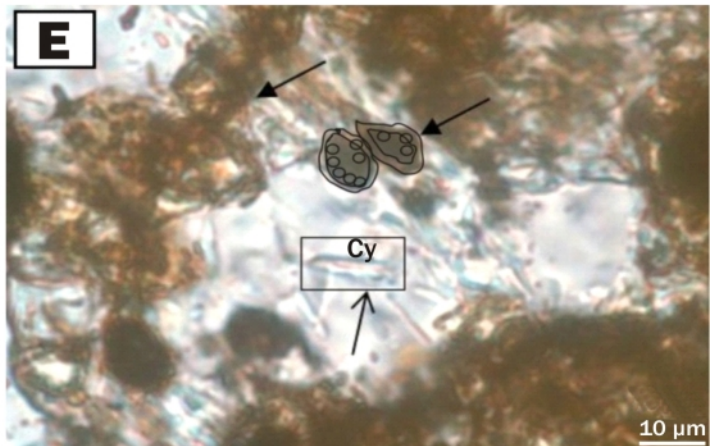
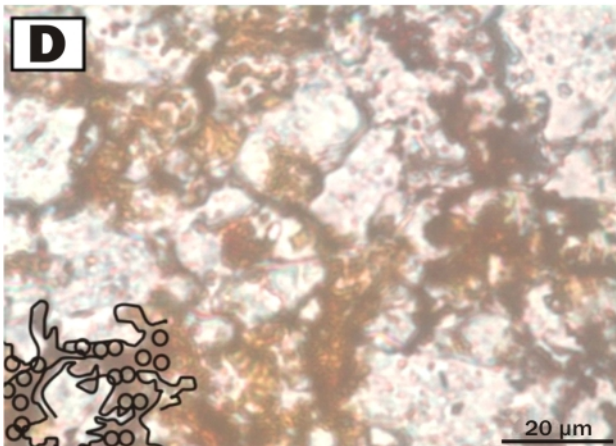
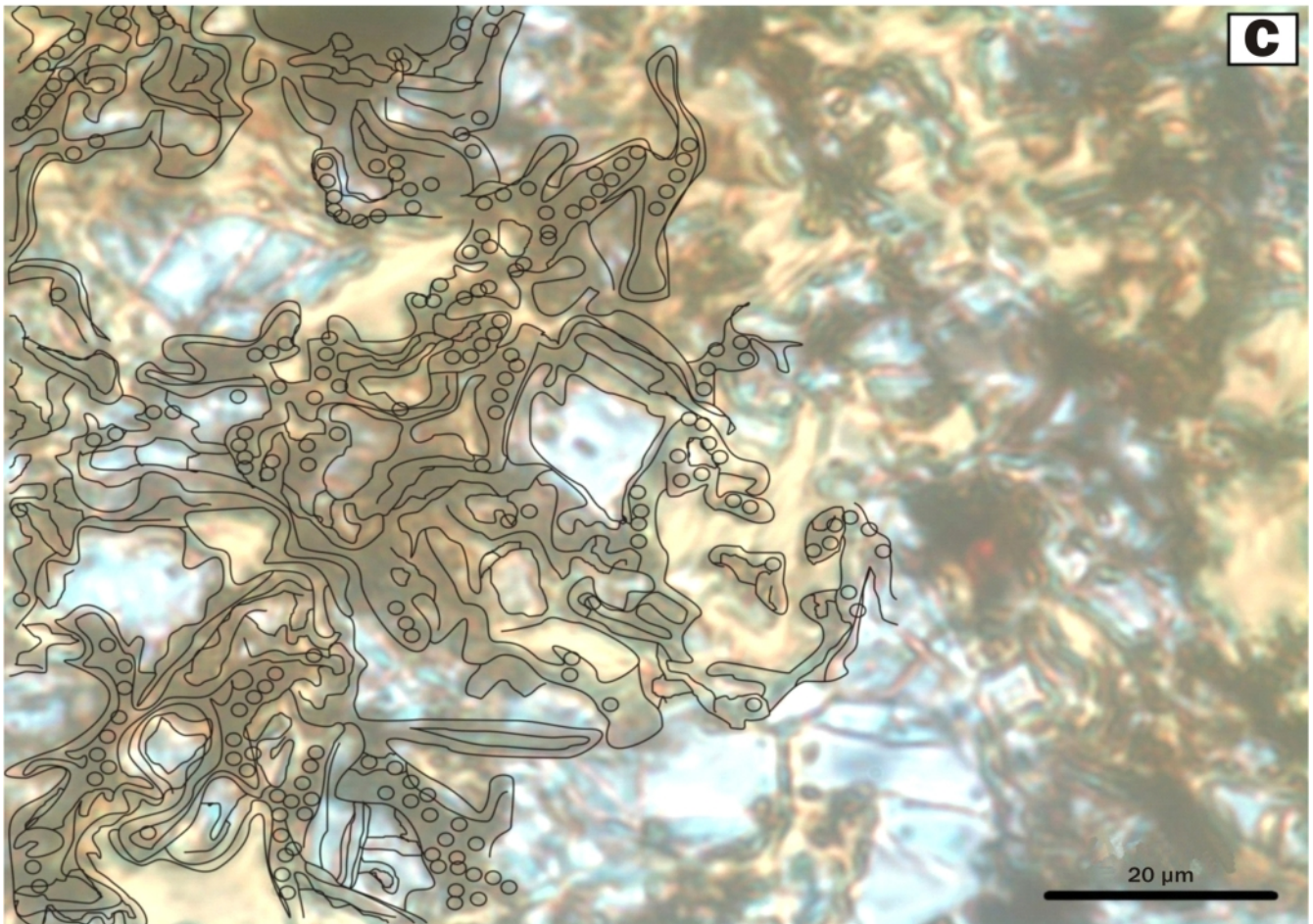
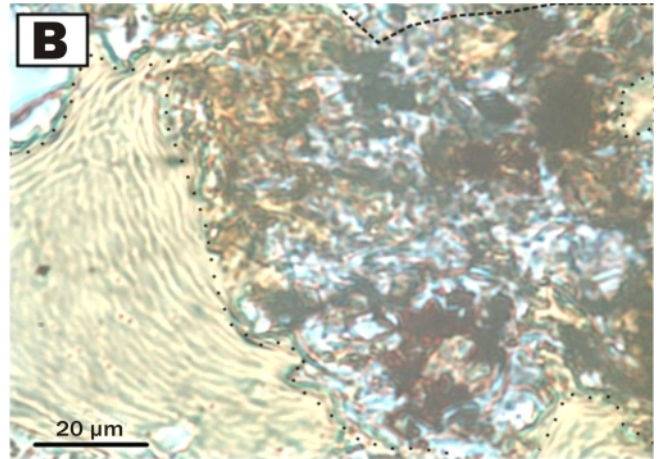
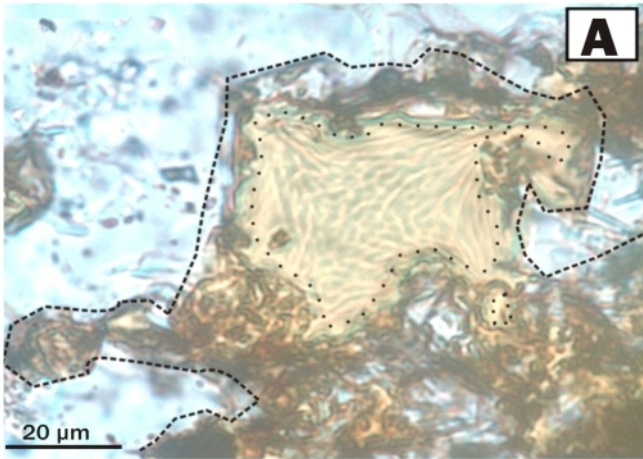


Figure 3: Biolumination in K2 profile (marked by black rectangles), where black points are pyrite (marked by arrows) (A, B, thin section photos). (A): Biolumination occurs at the upper part. (B): Biolumination occurs at the bottom part of the thin section. (C): Enlarged area of biolumination is marked by a white rectangle on (B) (optical microscopy, 1N, transmitted light).



higher density compared to surrounding micritic-clayey laminae. Sample K2 (platform facies/Ongongo) includes wavy laminated structures (Fig. 3C), wherein well-preserved coccoidal rusty bacterial colonies occur embedded in diagenetic quartz layers. More occurrences of these Type 1 microbial structures were found in sample K4-1 (platform facies/Entrance towards SW Valley), where microbial films are associated with detrital layers of micritic dolomite, and were also found in sample C1 (slope facies/Fransfontain), where dolomite layers are locally interspersed with syndimentary filamentous iron bacteria.

4.1.2 Type 2 microbial structures: Secondary biomats from biodegradation of iron-bearing minerals

Thin sections show a fabric-like lacework texture within the very fine-grained dolomite and quartz matrix, described as an interwoven, filamentous meshwork. The range of thicknesses of the mineralized filamentous structures is approximately 1-10 μm (Fig. 4A-E). The filaments are capped by a homogeneous mineral covering, generally goethite and rarely hematite, according to the Raman analyses. These intervals show diffuse contacts. The biomats are often so dense that they form an opaque mineralized segment (Fig. 4E). The matrix of the goethite and hematite structures consists of dolomite and/or quartz and organic matter as the main components. Filamentous forms of colonial coccoid cells, sheath-enclosed colonial unicells and spheroidal unicells also occur in the sections (Fig. 4DE). The presence of cyanobacteria with coexisting *Gallionella*-like Fe oxidizing bacteria supports shallow water conditions (Fig. 4E).

A carbonate-dominated debris flow deposit stands for the postglacial transition in the distal slope facies zone at Nara-chamspas locality, where a 20-cm-thick interval immediately overlying the Ghaub diamictite deposit was studied (sample C2a). Herein, the lower part (sample section C2a, 1-3 subsamples) contains debris-bearing layers composed of coarse-grained carbonate, microcline and quartz. Sigma clast quartz grains suggest a tectonic origin for a part of the debris (Gyollai et al. 2014b). In the upper part of the profile (sample section C2a, 4-7 subsamples), the debris flow contains quartz sand lenses (Fig. 2B), and altered chlorite (Fig 4A-C) and pyrite (Fig. 5A-D). The chlorite grains (60 μm in size) are kinked due to later tectonic deformation. These chlorite grains are reworked at rim by iron-oxidizing bacteria, more of them at inner parts of grains as well. Rapid chemical oxidation of the

Figure 4: Bio-weathering of chlorite (optical microscopy, 1N, transmitted light). Bioweathering of detrital kinked chlorite in profile C2a, where the biodegradation rim is marked by a dashed line (A, B, C), relict chlorite remnants are marked by pointed line. The rusty bacterial colonies are partly enhanced by the drawing for easier recognition (C). (D-E): Rusty bacterial colonies in carbonates in profile C2a partly outlined by the drawing for easier recognition. The meshwork is composed by coccoidal-amoeboid communities shown by arrows, well-preserved cyanobacteria is marked by black rectangle (Cy), and filamentous, carpet-like network also indicated by arrow.

transition layer was not observed. Quartz often encloses structures of cyanobacteria (Fig. 4E). Small, cubic pyrite grains show concentric growth rims, whereas larger pyrite grains are framed with layered, paragenetic lepidocrocite. Within the Khovarib fold belt, sample K4 (Entrance towards SW Valley) represents the Marinoan boundary contact in platform facies lithologies; thin red-green marly micrite marks the direct boundary between diamictite and cap dolomite, the latter being reddish stained by oxidized iron at its basal layer. Lenticular aggregates composed of pyrite and quartz are contained in these very basal cap carbonate layers (Keilberg Mb.) in which the grains are characteristically rimmed with iron-oxide. Visible components of filamentous rusty bacteria may have contributed to the degradation process of pyrite grains (Fig. 2D, Fig. 5BC). Hence, the rusty microbial communities occur as small, isolated groups inside the decayed grains, at the grain boundaries (ghosts), or along fractures (Fig. 4D).

4.1.3 Type 3 microbial structures: „Pseudo-secondary” structures coating on clasts

Filamentous rusty bacterial colonies were observed growing on carbonate clasts of the topmost diamictite layer in platform facies environments at Entrance towards SW Valley (sample C14a) (Fig. 6).

4.2 Raman-mapping measurements

According to reflectance microscopy and micro-Raman mapping, the pyrite altered to variable secondary minerals, such as hematite, goethite-lepidocrocite, and carbonaceous material (sample K4, Entrance towards SW Valley). In general, the altered pyrite has a remnant phase in the core zone, which is surrounded by a lepidocrocite-goethite-hematite alteration zone (Fig. 7). The microtexture of these minerals shows a fine, micro-layered structure, interbedded with organic material, resembling to *Gallionella/Mariprofundus*-like filamentous bio-signatures (Chan et al., 2011; Konhauser, 2012).

4.3 Geochemistry

Selected trace element and Fe composition are summarized in Table 2 for profile K4, and Fig. 8AB for profiles K2 and C2a. Highly elevated Fe content occurs at the basal samples in section K4 (K4-1, -2 subsamples). Elevated values of Co, Ni, and Zn with slightly negative $\delta^{13}\text{C}$ anomalies in profile K2 (5-8 subsamples) and the strongly negative $\delta^{13}\text{C}$ anomalies and elevated Ni in range of K2-2 subsample were observed (Fig. 8A). In profile C2a within profile C2a-12-15 subsample interval, near to the visible biodegradation of detrital mineral grains accumulated in lenses, elevated trace element contents of Ba, Sr, Co, Ni, Zn, Ce, and As occur (Fig. 8B).

Enrichment factors (EF, i.e., the abundances of biogenic elements divided by the Sc abundance, e.g., Meyer et al., 2012) were used for the determination of biogenic signatures (Table 3 for profiles K2, K4, and C2a). Because of the lack of Al data for most samples, Sc was used for normalization of detrital source effects.

The measured iron-rich biomat layers show high EF for Co, Ni, Zn, Fe, and U in the profiles K2 and K4, but the profile C2a has a higher EF only for Ni, and somewhat less for Co, whereas the other elements have normal marine values (0.5-2.0). The carbon isotopic ratios show a negative shift in profile K2

from about -8 ‰ (1-5 subsamples) to about -3 ‰ (6-11 subsamples)(Fig. 8A), and ranging -1 and -2 ‰ for profile K4 (Table 2).

Paleoredox indicators, such as U/Th (Yang et al., 2011), V/Cr, and V/(V+Ni) (Rimmer (2004), are given in Table 4. For U/Th the

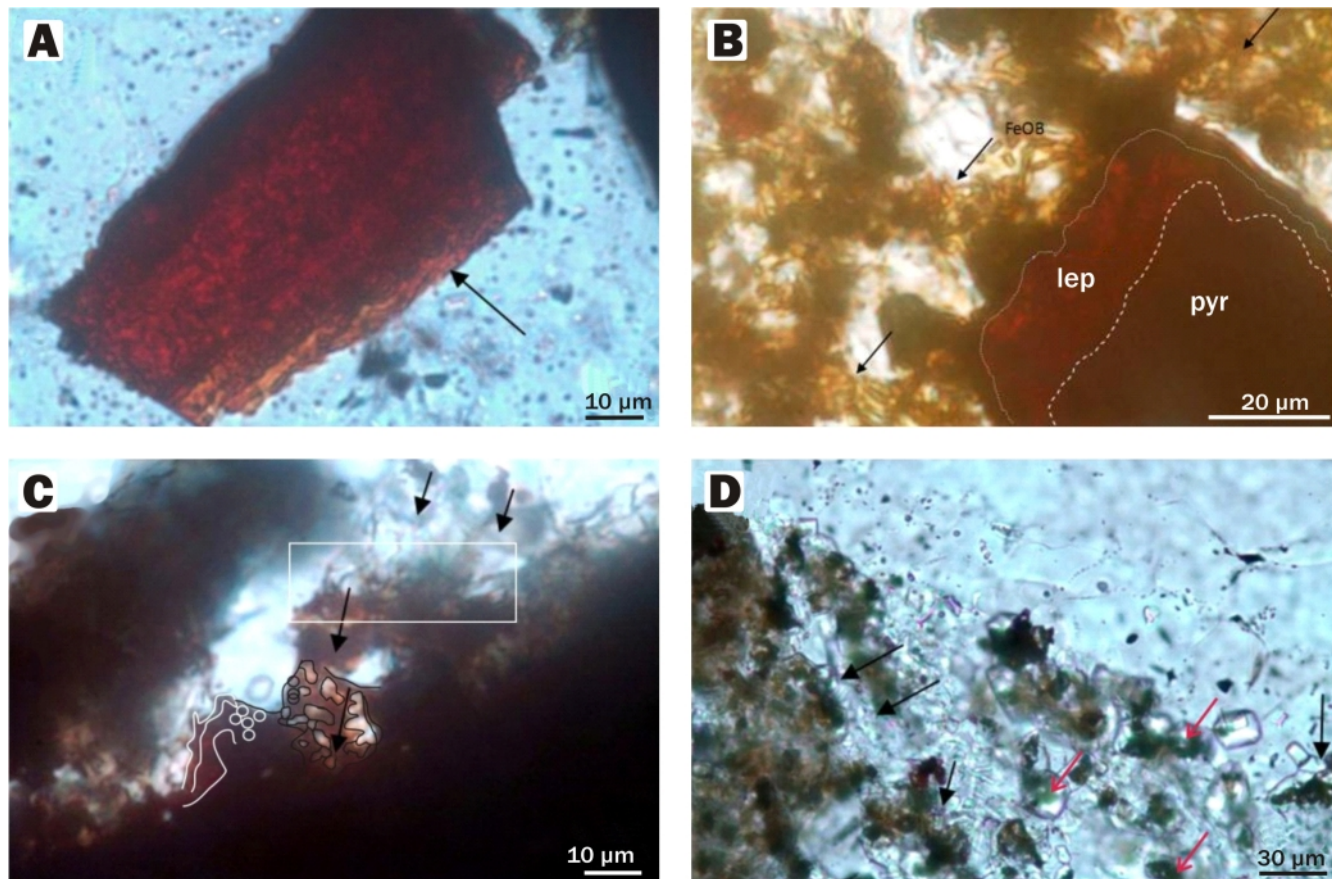


Figure 5: Bioweathering of pyrite in profiles K2 and K4. (A-B): Pyrite altered to goethite and lepidocrocite due to biodegradation (mineralogy is according to Raman spectroscopy; lep-lepidocrocite, pyr-pyrite, FeOB-Fe oxidizing bacteria showed also by arrows, dashed line shows the border between pyrite and lepidocrocite, thin line shows outer rim of lepidocrocite). (C) Coccoidal bacteria, marked by white circles, and carpet-like bacterial network preserving original form of pyrite (marked by black and white lines and arrows), bacterial filaments are marked by white rectangle). (D): Rusty bacteria (indicated by black arrows), which started to alter to green clay (indicated by red arrows).

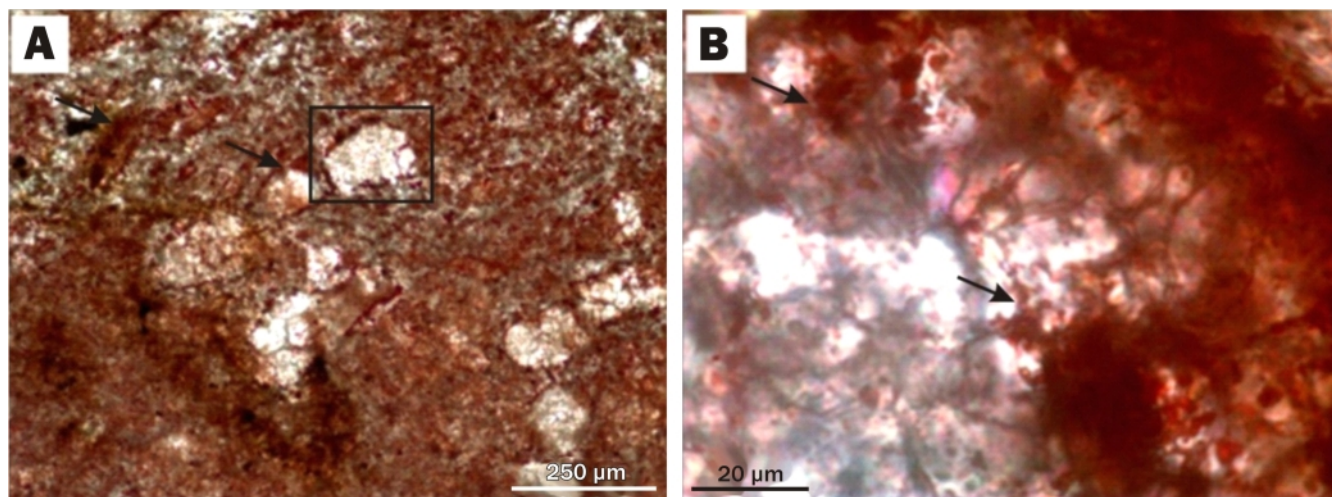


Figure 6: Microbial mats on the clasts in sample C14a. (A): A coated clast is marked by black rectangle. (B): Fe-rich-mats are marked by arrows (optical microscopy, 1N, transmitted light).

value <0.75 refer to oxic, values between 0.75-1.25 to suboxic, and >1.25 to anoxic conditions. In the case of V/Cr, the value <2.0 refer to oxic, values between 2.0-4.25 to suboxic, and >4.25 to anoxic conditions. For V/(V+Ni), the value <0.46 refer to oxic, values between 0.45-0.6 to suboxic, and >0.54 to anoxic conditions. Our results show oxic-suboxic conditions for most of the samples based on these proxies.

Location Strat. setting wt. %	Entrance towards SW Valley							
	G/M*	G/M	M	M	M	M	M	M
	K4-1	K4-2	K4-3	K4-4	K4-5	K4-6	K4-7	K4-8
Fe ₂ O ₃	9.05	2.22	0.48	0.44	0.45	0.47	0.50	0.45
ppm								
Cr	16.9	5.22	4.54	3.05	3.68	6.10	3.85	3.30
Co	38.5	6.45	2.39	2.01	1.88	2.20	2.41	2.06
Ni	89.1	16.5	11.1	4.88	8.93	11.9	11.8	4.75
Zn	50.1	26.4	22.5	21.5	22.5	29.7	23.6	20.6
As	28.1	6.93	0.62	0.48	0.45	0.44	0.65	0.55
Rb	8.61	6.74	6.35	5.55	5.58	7.5	6.73	5.71
Sr	60.7	56.7	68.2	62.8	64.3	64.3	67.5	62.1
Zr	<28	39.6	27.9	21.1	30.4	30.0	28.6	19.4
Ba	58.6	29.5	44.8	34.3	33.9	45.3	39.6	32.4
La	4.62	4.78	4.86	4.43	4.34	4.17	4.08	3.73
Ce	11.3	9.52	9.28	8.24	8.43	8.26	8.16	7.23
U	4.51	1.48	1.33	0.55	0.44	0.57	0.54	0.35
δ ¹³ C _{vs VPDB}	-0.95	-1.41	-1.91	-1.69	-1.87	-1.69	-1.84	-1.68

*G= Ghaub Fm., G/M= boundary, M=Maieberg Fm.

Table 2: Fe and selected trace element composition of samples from profile K4 (Entrance towards SW Valley)

5. Discussion

5.1 Microbial Fe(II) oxidation

The most prominent candidates for Fe-bearing mineral bio-weathering and biomineralization are prokaryotes (Konhauser, 1998; Ehrlich, 2015). Thus, we propose that mineralizing prokaryotes indicate microbial mediation, e.g., Fe-bacteria causing Fe-oxide biomineralization and a characteristic filamentous microstructure, together with organic matter.

Microbes living in the solution (aquatic environment) were mineralized and matrix minerals were precipitated in close connection with preserved microbes (authigenic mineralization). Some types of microbes form complex microtextural features (filamentous forms with inner globular fine texture), representing textural evidence for the presence of microbes (Figs. 3ABC). The homogeneous Fe precipitation along the filaments that build a 3D network is a robust biosignature (Chan et al., 2011). Similar mineralized structures were reported in the Sturtian Rasthof Formation by Gyollai et al. (2015). Understanding the biogeochemistry of biomat formation is the key for determining the type of Fe-rich biomats that may have been involved in the lithogenesis and thus are defining the suspected environmental conditions. There are four types of microbial metabolism that can oxidize Fe²⁺-forming Fe-oxide minerals (Konhauser, 2012). The first type of the microbial Fe(II) metabolisms is acidophilic and oxic, the occurrence of which in natural shallow fresh- to brackish-water conditions is unlikely. A second type of microbial Fe(II) metabolism is driven by light, anoxic/anaerobic, and neutrophilic (photoferrotroph); a condition that is not supported by the mineralogy here which contains smectite. The third type is suboxic/anaerobic, where neutrophilic NO₃ reducers coupled with Fe(II) oxidizers probably contributed to the biochemical milieu, but morphological features do not support this metabolism as main process in our Marinoan biomat formation. The formation conditions were thus most likely governed by the fourth type, namely suboxic and neutrophilic *Gallionella/Mari profundus*-like Fe-oxidizing microbes (*Gallionella*-brackish, *Mari profundus*-normal salinity conditions; Konhauser, 2012) based

on filament-forming microstructure. Non-enzymatic reactions provide an indirect role for bacteria in the oxidation of Fe. As a result of microbial activity, chemical conditions (Eh, pH) change in the vicinity of the cells, favoring the chemical oxidation of Fe. Non-Fe-oxidizing microbes may have been the sole microbiota involved in mat formation. The main difficulty with this scenario, however, is the uniformity of the Fe lace-work structures throughout the section, which would not be expected to form from inorganic processes.

5.2 Identification of biosignatures

The mineralized biosignatures, which have greater chance to survive over geological times if they are rapidly and extensively encrusted (like goethite after microbially produced ferrihydrite), represent opportunity to detect microbial mediation. Mineralogical studies confirmed the presence of Fe biominerals, such as ferrihydrite, lepidocrocite, goethite, and magnetite, similarly to occurrences reported by Fortin et al. (1997), Konhauser (1998) and Ehrlich (2015), confirming biogenicity. Variable organic matter constituents occurring in the microbial-like textures, as remnants of earlier microbial activity, were also found in our samples (Fig. 7), similarly to Molnár et al. (2017) and Rajzabadeh et al. (2017).

Therefore, morphology in combination with mineralogical and chemical bioindicators point towards a complex interpretation (Baele et al., 2008), with microtextural characteristics (filamentous, tubular, coccoidal forms of iron-oxide hydroxides), the carbon isotopic composition, and the bulk rock geochemical data support this scenario. The enrichment of some elements, such as Fe, P, Zn, and Mn, can be related to biogenic activity, similar to the presence of negative carbon isotopic signatures (Polgári et al., 2012ab).

5.3 Diagenesis of Fe-rich biomats

According to the diagenesis of Fe-rich biomats, the microbes produce poorly ordered ferrihydrite as a primary mineral, which transforms to more ordered minerals, such as goethite or hematite, within a few months or years via dissolution-dehydration processes (Konhauser, 1998; Schwertman and Cor-

nell, 2007). The main Fe oxide mineral in the filaments of our samples is goethite, but Raman analyses indicate that hematite is also present, similarly to those, reported by Rajabzadeh et al. (2017). The fossilized Fe-rich biomats were rapidly and extensively encrusted by authigenic minerals, such as dolomite and silica, similar to what has been reported by Baele et al. (2008). The amorphous silica can easily be transformed into more stable minerals, such as cristobalite, tridymite, and quartz (Herdianita et al., 2000). Silica precipitation is derived by either the destruction of organic complexes or the transformation of ferrihydrite (Baele et al., 2008). Muscovite (hydro-muscovite) is common in the studied samples and was most likely formed by the diagenesis of cyanobacteria filaments in Fe-rich microbialites by the leaching of biofilm alkali elements (Na, K, Al, Mg) as reported by Ewers (1983).

5.4 Geochemistry of biomats

Microbial structures can be identified not only by their mineralogy and texture, but also by their geochemistry. Enzy-

matic activity causes the enrichment of the so-called biophilic elements, such as Zn, Ni, and Co. In addition, there are microbes that form large mineral deposits, such as manganese-oxidizing bacteria (they also oxidize and selectively enrich Co and Ce); iron-oxidizing bacteria form Fe-oxide enrichments (also deposits), etc. (Polgári et al., 2012ab). These microbes sequester metals from solution to the solid phase. The detected anomalies in Fe, Mn, Mg, Co, Ni, Cu, Zn, and Mo can be correlated to microbial activity (Takahashi et al., 2007). The enrichments of some major elements (Al, Si, Na, Ca, Mg), the REE and other trace elements (Y, Zr, Nb, Hf, Pb, Th) belong to an early phase (lag-log phase) of the Fe-oxidizing microbial processes via bacteria (Gallionella) (Heim, 2010).

The elevated contents of Co, Ni, and Zn and slightly negative $\delta^{13}\text{C}$ anomalies (bulk) in the range of our profile K2 (05-08 subsamples) can probably be attributed to microbial metabolism (Fig. 7). The slightly negative $\delta^{13}\text{C}$ anomalies and elevated Ni indicate aged biomats in the basal part of our profile K2 (01-03 subsamples) (Fig. 7). Similarly, in our profile C2a,

EF	K2-	K2-	K2	K2-	K4-	K4-	K4-	K4-	K4-	K4-	K4-	K4-							
	1	2	-3	4	5	6	7	8	9	10	11	1	2	3	4	5	6	7	8
Cr	1.2	1.2	1.3	1.1	0.9	0.3	0.5	0.4	0.5	0.4	0.7	1.4	1.0	0.8	0.7	0.7	0.9	0.6	0.6
Co	0.2	0.1	0.1	0.0	0.3	2.4	6.8	3.8	1.5	2.1	1.4	14.7	6.1	2.1	2.1	1.8	1.5	1.9	1.8
Ni	0.7	0.9	0.5	0.3	1.8	3.0	7.8	4.3	2.5	2.5	2.5	14.3	6.5	4.0	2.2	3.5	3.3	3.9	1.7
Zn	0.5	0.5	0.4	0.5	0.6	1.2	3.9	2.5	2.4	2.8	2.9	5.2	6.8	5.3	6.2	5.5	5.4	5.0	4.8
Rb	1.1	1.1	1.1	1.0	1.3	0.4	0.5	0.5	0.5	0.4	0.6	0.5	0.9	0.8	0.8	0.8	0.7	0.8	0.7
U	2.7	2.8	2.8	2.5	5.6	2.8	5.0	3.2	2.1	3.0	2.7	12.8	10.4	8.6	4.3	3.1	2.8	3.1	2.2
K	1.8	1.8	1.8	1.9	2.2	0.6	0.6	0.8	0.8	0.8	1.0	0.6	1.1	1.5	1.7	1.6	1.4	1.7	1.5
Fe	0.4	0.4	0.3	0.2	1.7	1.7	2.4	1.3	0.9	1.4	1.0	11.0	6.7	1.3	1.5	1.3	1.0	1.3	1.2

EF	C2a	C2a-	C2a-	C2a-	C2a-	C2a-	C2a-	C2a-	C2a-	C2a-	C2a-	C2a-	C2a-	C2a-	C2a-	C2a-	C2a-
	1	2	3	4	5	6	7	8	9	10	11	12	13	14	15	16	17
Cr	1.2	0.6	0.6	0.5	0.5	0.5	0.5	0.5	0.6	0.5	0.5	0.5	0.5	0.5	0.5	0.6	0.6
Co	0.7	0.5	0.4	0.9	0.4	0.4	0.4	0.4	1.1	0.4	0.6	0.5	0.8	1.4	0.8	2.4	4.3
Ni	2.0	2.1	2.3	3.4	2.2	2.0	2.1	1.8	1.9	1.8	2.0	2.0	2.9	4.5	1.8	3.7	9.7
Zn	0.4	0.6	0.5	0.6	0.6	0.6	0.7	0.6	0.6	0.6	0.6	0.6	0.6	0.6	0.7	0.9	1.9
Rb	0.6	0.5	0.7	0.6	0.6	0.6	0.7	0.5	0.6	0.6	0.6	0.7	0.7	0.7	0.6	0.7	0.7
U	0.6	0.6	0.7	0.6	0.6	0.6	0.7	0.6	0.7	0.7	0.6	0.8	0.7	1.0	0.7	1.0	1.0
K	1.0	0.8	1.2	1.1	1.1	1.0	1.1	1.0	1.2	1.2	1.0	1.2	1.1	1.3	1.1	1.1	0.8
Fe	0.3	0.3	0.3	0.4	0.4	0.5	0.5	0.5	0.6	0.5	0.5	0.5	0.6	0.9	0.6	1.1	1.2

* Calculation of EF was made after (Williams et al., 1995), enrichment caused by biogenic structures is marked by bold letters. For locality see Fig. 1.

Table 3: Enrichment factors (EF) of biogenic elements in K2 (Warmquelle), K4 (Entrance towards SW Valley) and C2a (Narachaamspos) profiles*

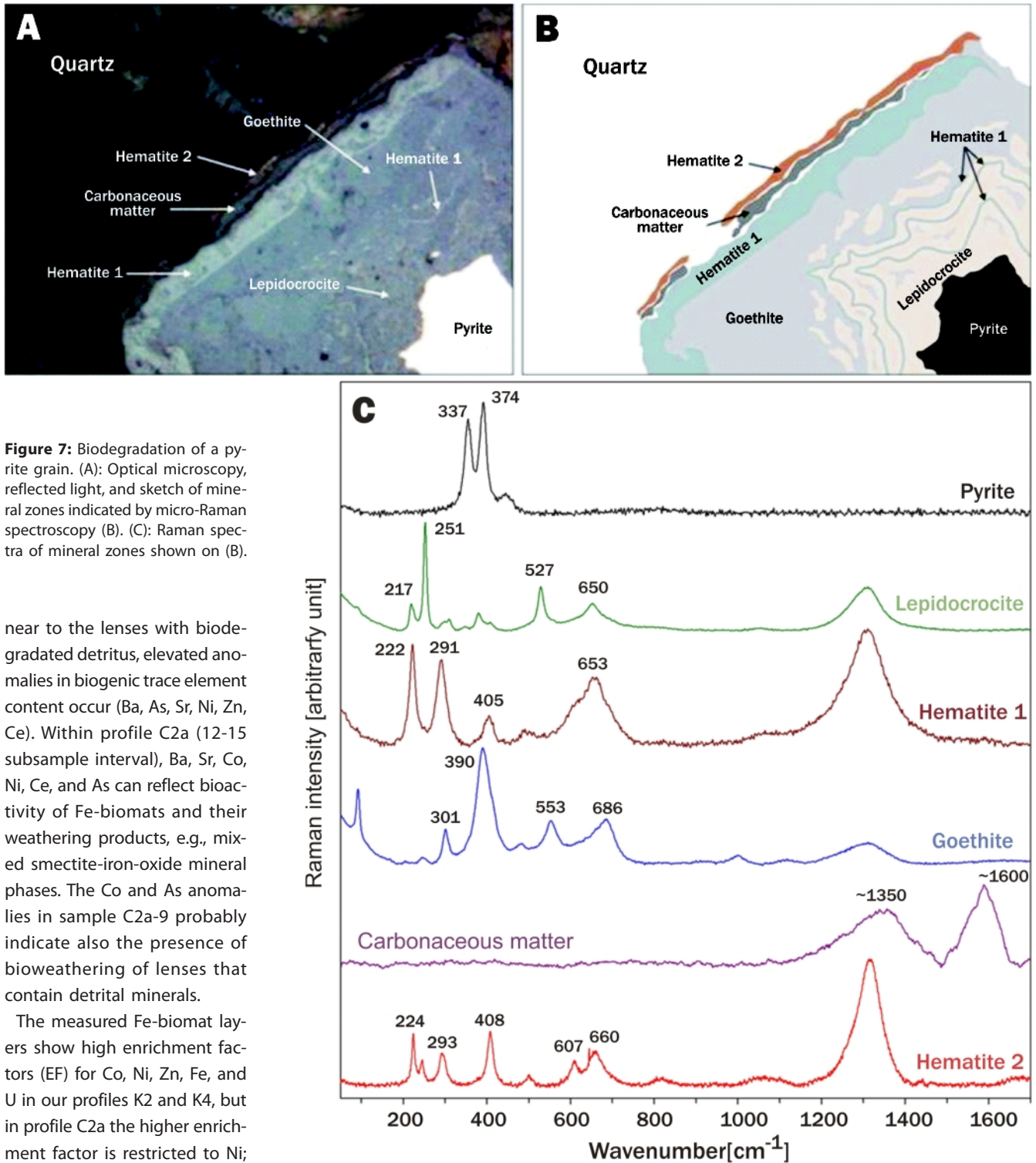


Figure 7: Biodegradation of a pyrite grain. (A): Optical microscopy, reflected light, and sketch of mineral zones indicated by micro-Raman spectroscopy (B). (C): Raman spectra of mineral zones shown on (B).

near to the lenses with biodegraded detritus, elevated anomalies in biogenic trace element content occur (Ba, As, Sr, Ni, Zn, Ce). Within profile C2a (12-15 subsample interval), Ba, Sr, Co, Ni, Ce, and As can reflect bioactivity of Fe-biomats and their weathering products, e.g., mixed smectite-iron-oxide mineral phases. The Co and As anomalies in sample C2a-9 probably indicate also the presence of bioweathering of lenses that contain detrital minerals.

The measured Fe-biomaat layers show high enrichment factors (EF) for Co, Ni, Zn, Fe, and U in our profiles K2 and K4, but in profile C2a the higher enrichment factor is restricted to Ni; the other elements have normal marine values (0.5-2.0)(Table 3).

5.5 Constraints on paleoenvironment and source of Fe

The Neoproterozoic oceans were fully oxygenated, which resulted in the decrease of dissolved Fe^{2+} in the water column and restricted Fe-oxidizing bacteria to the shallow water environment (Dahanayake and Krumbein, 1986) on the different metal sources.

During the Neoproterozoic, local hydrothermal activity could

have been the nutrient source for the iron oxidizing bacteria, and may have resulted in some cm-thick 3D structure of iron-oxidizing biomats, similar to those described from modern hydrothermal systems (Reysenbach and Cady, 2001; Campbell and Squire, 2010). Such features were observed in thin sections from the iron-rich Marinoan postglacial transition at Ongongo (profile K2) and Entrance towards the SW Valley (profile K4). The K2 and K4 samples have a laminated appearance of Gallionella-like fossil assemblages. The most proba-

Sampling site	Fransfontein		Narachaamspos		Tweelingskop		Bethanis		Entrance towards SW Valley		Khowarib Valley		Warmquelle		Narachaamspos																																																																														
	M	G/M	G/M	G/M	G	G	M	G	G	G	M	M	M	G/M	G/M	G	M																																																																												
Stratigraphy*	C1a	C1b	C1c	C2a	C2b	C2c	C3_1	C3_2	C4	C5	C6	C7	C14a	C14b	C14c	C14d	C14e	C14f	C14g	C14h	C14i	C14j	C14k	C14l	C14m	C14n	C14o	C14p	C14q	C14r	C14s	C14t	C14u	C14v	C14w	C14x	C14y	C14z	C15a	C15b	C15c	C15d	C15e	C15f	C15g	C15h	C15i	C15j	C15k	C15l	C15m	C15n	C15o	C15p	C15q	C15r	C15s	C15t	C15u	C15v	C15w	C15x	C15y	C15z	C16a	C16b	C16c	C16d	C16e	C16f	C16g	C16h	C16i	C16j	C16k	C16l	C16m	C16n	C16o	C16p	C16q	C16r	C16s	C16t	C16u	C16v	C16w	C16x	C16y	C16z	C17a	C17b	C17c
ppm/ppm	2.38	0.61	0.50	0.22	0.20	0.31	0.32	0.40	0.66	15.8	0.53	0.24	0.74	4.79	0.62	0.45	1.36	0.39	4.27	0.57	0.80	0.41	0.45	0.44	0.60	0.89	0.57	0.33	0.27	0.26																																																															
U/Th	0.03	3.24	1.85	1.08	0.80	1.44	2.17	2.11	1.59	6.53	1.02	1.16	1.91	0.53	1.97	2.11	n.d.	n.d.	1.95	1.15	0.94	1.64	n.d.	24.0	1.62	1.15	1.62	0.91	1.31																																																																
V/Cr	0.03	0.51	0.41	0.19	0.28	0.28	0.54	0.47	0.76	0.74	0.30	0.40	0.70	0.29	0.67	0.67	n.d.	n.d.	0.46	0.73	0.50	0.75	n.d.	n.d.	0.80	0.61	0.89	0.78	0.70																																																																
V/(V+Ni)																																																																																													

*G= Ghaub Fm., G/M= boundary, M=Maieberg Fm.; n.d. no data; U/Th calculated after Yang et al. (2011); V/Cr and V/(V+Ni) calculated after Rimmer (2004)

Table 4: Geochemical calculations for paleoenvironmental conditions

ble nutrient source in these cases could be hydrothermal, based on microbiological observations similarly to Sturtian Rasthof Fm. (Gyollai et al., 2015). Similar to sample C2a, the laminated structures in our sample K2 might also be formed by biodegradation of iron-rich minerals, whose precursor minerals were observed as pseudomorphic grain rims.

On account of restricted Fe and P input, mat building appeared temporary as thin laminae

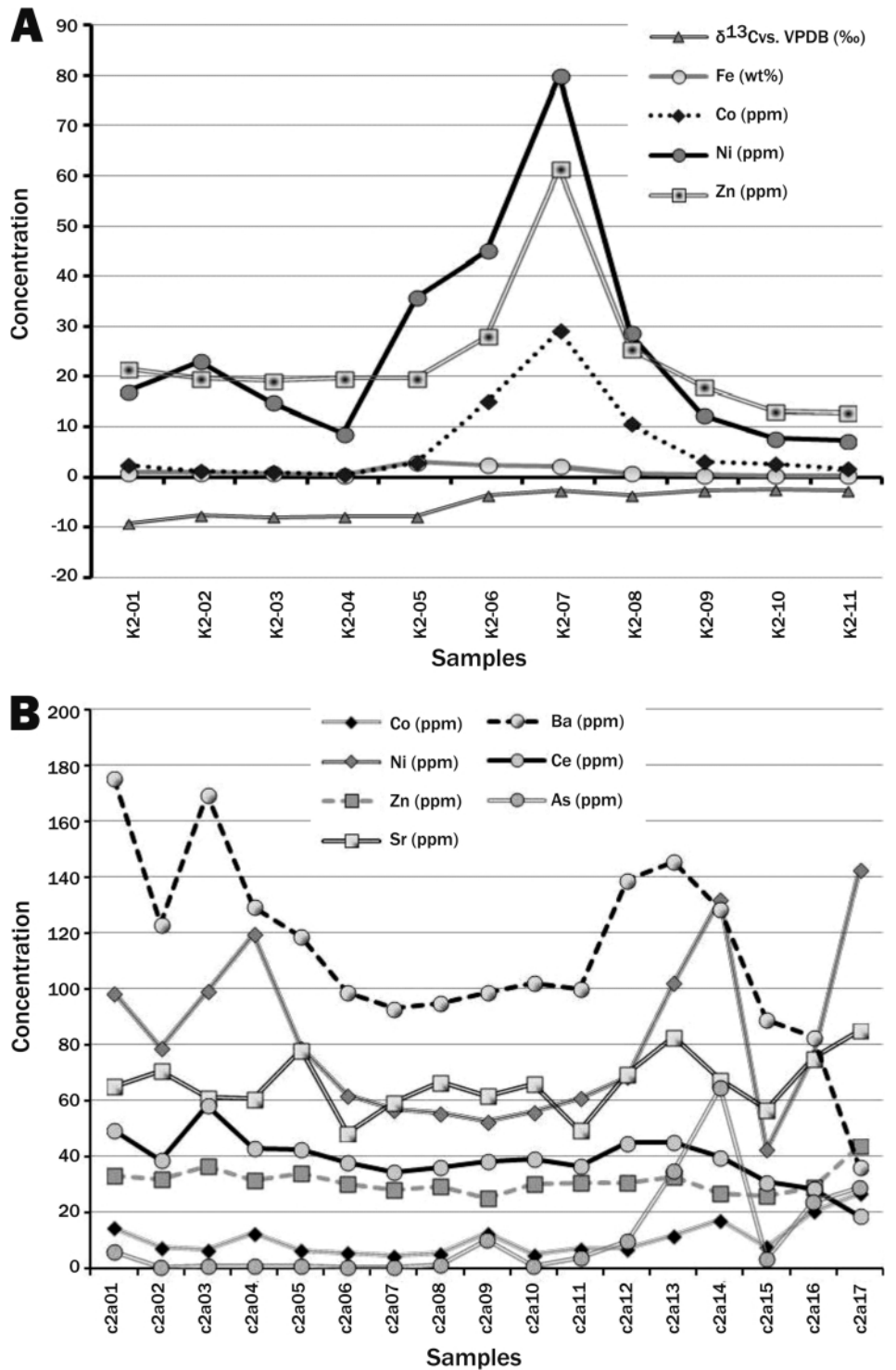


Figure 8: Distribution of biogenic element abundances in the profiles K2 (A) and C2a (B), indicating the enrichments of biogenic elements. (A): The more negative carbon isotopic anomaly correlates well with higher Ni abundances. The red microbialite region (profile K2 05-08 subsamples) is enriched in biogenic elements, such as Zn, Ni, and Co, to their abiogenic values. (B): Biogenic element accumulation (Co, Ni, Zn, As, Sr, Ba, Ce) follows distribution of pyrite-chlorite-quartz rich lenses. The two graphs represent two profiles; the first one is K2 with 11 subsamples, the other one is C2a with 17 subsamples.

(C1, Fransfontain) and coatings (C14a, Entrance towards SW Valley). The growth of iron bacteria on clasts suggests a short-term nutrient source or transient suboxic condition. The microstructure show extracellular polymeric substance (EPS)-like microlayered appearance (Fig. 3). Light $\delta^{13}\text{C}$ can also raise microbial mediation similarly to recent and ancient terrestrial occurrences (Fortin et al., 1997; Polgári et al., 2012a).

Probably a short-term iron source solved the nutrient source for filamentous iron bacteria, which development ended either by suboxic conditions turned to more oxic or abrupt arrival of iron-hydrothermal fluids. Paleoproxy indicators support this scenario (Table 4), but great care has to be taken in the complex interpretation of the data in such microbially mediated systems (Bíró et al., 2015).

All Fe(II)-bearing minerals are possible nutrient sources for Fe-oxidizing microbes in perfect conditions (suboxic and neutral for most FeOB). The presence of sigma clasts suggests pressure-dominated metamorphism after initial bioweathering in profile C2a (Gyollai et al., 2014b). Sigma clasts of quartz and pyrite confirm the formation of pyrite via precipitation from hydrothermal solutions during a shear-tectonic event. However, the pyrite could be detrital origin, but coexistence with sigma clast quartz suggests a tectonic origin.

The biodegradation of pyrite is either due to surface weathering or happened earlier under low metamorphic conditions after a later tectonic event, for example, the collision of the Congo Craton with the active margin of Rio de la Plata Craton (630-550 Ma), which induced the formation of the Pan-african orogenic belts (Stanistreet et al., 1991; Alkmim et al., 2001). Pyrite and chlorite provided the nutrient source for the growth of filamentous iron bacteria by secondary biomats. The biodegradation (alteration) and biomineralization just in the vicinity or at the same place can be characteristic in the form of Fe-oxide minerals - the so called „bioindicator“ minerals, such as ferrihydrite (transforming very quickly to more stable goethite), hematite (depending on the conditions), and lepidocrocite. The pyrite in profile C2a (thin sections C2a-4-7) was oxidized by microbial degradation, which is indicated by a lepidocrocite and hematite rim surrounding a pyrite core (Fig. 7). The hematite could be a simple weathering product (sample C7, Bethanis) or the result of complex bioweathering (sample P49-1). Pyrite and chlorite provided the nutrient source for the growth of filamentous rusty bacteria. The *Gallionella*-like microfossils occur in the erosion rim of chlorite and in degradation cavities, which provide the iron-bearing minerals as a source of nutrients in C2a (Narachaamspos sample), similar to what was proposed by Hoffman et al. (1998b, 2011).

In general, Fe-rich biomats are encrusted by dolomite and silica (Baele et al., 2008), which is also present in our samples. Fe-rich biomats are better preserved in diagenetic quartz, than in carbonate host material, which is well documented in our profile C2a.

Regardless of geological age and geographical location, the Fe-rich structures associated with microbes and paleoenvironments always witness gradients of oxygen and Fe^{2+} along

various mineral interfaces (Preat et al., 2000; Konhauser et al., 2002). Bacterial cells can precipitate a wide variety of Fe minerals through variable metabolic processes (Konhauser, 1998).

Microbial mats in our studied transition layers, situated between glacial Ghaub Diamictite and post-glacial Maieberg cap carbonate, trapped sedimentary particles on the one hand, but also caused biodegradation of detrital mineral components in the course of successive mineral diagenesis. Thus, brackish water conditions, due to sea level rise in postglacial periods, must have dominated wide areas of the Otavi platform during the tested period. This bacterial growth may suggest that environmental conditions of the postglacial period were established shortly after the cessation of diamictite deposition.

6. Conclusions

The synsedimentary mats of platform facies formed within neutrophilic suboxic conditions, specific for starving basin environments, where the nutrient presumably came from the input of hydrothermal vents. In contrast, the nutrients of secondary microbial mats were iron-bearing minerals, such as chlorite and pyrite. The coating of iron-oxidizing bacteria on clast surfaces indicate transient suboxic conditions that subsequently turned to oxygenic conditions. The presence of smectite (montmorillonite) in microbial mats indicates oxygenic conditions, as well as the paleoredox indicator proxies during formation and diagenesis. These Fe-oxidizing bacterial biosignatures represent important information on the oxygen supply of the synsedimentary environment and support the oxygenation of the seawater via sea level rise caused by melting ice.

Pyrite sigma clasts sheeted with quartz fibers indicate tectonic shearing during diagenesis or a later low grade metamorphic process, which affected the deposits of our research area due to the subsequent Panafrican Orogeny.

Acknowledgements

We are grateful to Dieter Mader (INAA), Peter Nagl (XRF), and Susanne Gier (XRD) for assistance in lab work and helpful discussions. This study was supported by the Austrian Academy of Sciences through a grant to one of us (C. Koeberl) through the International Geological Correlation Program IGCP No. 512 of the Austrian Academy of Sciences. The samples were collected by one of us (F. Popp), supported by the Geological Survey of Namibia and its Director Dr. G. Schneider, to whom we are grateful for important logistical support. We appreciate the help of the reactor team of the Institute of Atomic and Subatomic Physics (“Atominstitut”), Vienna, with the irradiations. We thank for the constructive comments of the Editor in Chief and reviewer Gerd Winterleitner.

References

- Alkmim, F.F., Marshak, S. and Fonseca, M.A., 2001. Assembling West Gondwana in the Neoproterozoic: Clues from the Sao Francisco craton region, Brazil. *Geology*, 29, 319-322.
- Baele, J.-M., Bouvain, F., De Jong, J., Matielli, N., Papier, S. and Prat, A., 2008. Iron microbial mats in modern and Phanerozoic environments. *Proceedings of SPIE - The International Society for Optical Engineering*, 7097, 70970N-70970N-12. <http://dx.doi.org/10.1117/12.801597>
- Bechstadt, T., Jager, H., Spence Werner, G., 2009. Late Cryogenian (Neoproterozoic) glacial and post-glacial successions at the southern margin of the Congo Craton, northern Namibia: facies, palaeogeography and hydrocarbon perspective. *Geological Society, London, Special Publications*, 326, 255-287.
- Biro, L., Polgari M, M Toth, T., Vigh, T., Kavasi, N. and Sahoo, S. K., 2015. Terrestrial radioisotopes as paleoenvironmental proxies in sedimentary formations. *Journal of Radioanalytical and Nuclear Chemistry*, 306, 1, 289-293. <http://dx.doi.org/10.1007/s10967-014-3861-z>
- Campbell, I.H. and Squire, R.J., 2010. The mountains that triggered the Late Neoproterozoic increase in oxygen: the second great oxidation event. *Geochimica et Cosmochimica Acta*, 74, 4187-4206. <http://dx.doi.org/10.1016/j.gca.2010.04.064>
- Chan, C.S., Fakra, S.C., Emerson, D., Fleming, E.J. and Edwards, K.J., 2011. Lithotrophic iron-oxidizing bacteria produce organic stalks to control mineral growth: Implications for bio-signature formation. *The International Society for Microbial Ecology Journal*, 5, 717-727. doi:10.1038/ismej.2010.173. <http://dx.doi.org/10.1038/ismej.2010.173>
- Coplen, T., Brand, W., Gehre, M., Groning, M., Meijer, H., Toman, B. and Verkouteren, R., 2006. New guidelines for $\delta^{13}\text{C}$ measurements. *Analytical Chemistry*, 78, 2439-2441. <http://dx.doi.org/10.1021/ac052027c>
- Dahanayake, K. and Krumbein, W.E., 1986. Microbial structures in oolitic iron formations. *Mineralium Deposita*, 21, 85-94.
- Domack, E. and Hoffman, P., 2003. Stratigraphic transition into and out of Snowball Glacial: Evidence from the Otavi Platform and Fransfontain slope, Namibia. *Eos Transactions American Geoscience Union*, 84/46, Fall Meeting Supplement, Abstract C11B-0819.
- Domack, E. W. and Hoffman, P.F., 2011. An ice grounding-line wedge from the Ghaub glaciation (635 Ma) on the distal foreslope of the Otavi carbonate platform, Namibia, and its bearing on the snowball Earth hypothesis. *Geological Society of America Bulletin*, 123/7-8, 1448-1477. <http://dx.doi.org/10.1130/B30217.1>
- Ehrlich, D., 2015. *Geomicrobiology 6th* (Ed.), Marcel Dekker, New York 635 pp.
- Ewers, W.E., 1983. Chemical Factors in the Deposition and Diagenesis of Banded Iron-Formation, in: A.F. Trendall and R.C. Morris (Eds.): *Developments in Precambrian Geology*, 6, Iron formation: Facts and Problems. Elsevier, pp. 491-512.
- Eyles, N. and Januszczak, N., 2004. 'Zipper-rift': a tectonic model for Neoproterozoic glaciations during the breakup of Rodinia after 750 Ma. *Earth-Science Reviews*, 65, 1-73. [https://doi.org/10.1016/S0012-8252\(03\)00080-1](https://doi.org/10.1016/S0012-8252(03)00080-1)
- Fairchild, I. J. and Kennedy, M. J., 2007. Neoproterozoic glaciation in the Earth System. *Journal of Geological Society London*, 164, 895-921. <http://dx.doi.org/10.1144/0016-76492006-191>
- Fortin, D., Ferris, F.G. and Beveridge, T.J., 1997. Surface-mediated mineral development by bacteria. *Reviews of Mineralogy*, 35, 161-180.
- Fraiser, M.L. and Corsetti, C.A., 2003. Neoproterozoic Carbonate Shrubs: Interplay of Microbial Activity and Unusual Environmental Conditions in Post-Snowball Earth Oceans. *Palaios*, 18, 378-387.
- Gaschnig, R.M., Rudnick, R.L., McDonough, W.F., Kaufman, A. J., Hu, Z. and Gao, S., 2014. Onset of oxidative weathering of continents recorded in the geochemistry of ancient glacial diamictites. *Earth and Planetary Science Letters*, 408, 87-99. <https://doi.org/10.1016/j.epsl.2014.10.002>
- Gyollai, I., Mader, D., Polgari, M., Popp, F. and Koeberl, C., 2014b. Lack of evidence for impact signatures in Neoproterozoic postglacial deposits from NW-Namibia. *Austrian Journal of Earth Sciences*, 102/2, 100-111.
- Gyollai, I., Polgari, M., Veres, M., Nagy, Sz., Popp, F., Mader, D. and Koeberl, C., 2014a. Evidence of microbial activity involved with Neoproterozoic postglacial sediments from the Otavi Group, Namibia: a study of Sturtian oolitic carbonate sandstone with spectroscopic methods. *Communications of the Geological Survey of Namibia*, 15, 117-133.
- Gyollai, I., Polgari, M., Fintor, K., Popp, F., Mader, D., Pal-Molnar, E., Nagy, Sz. and Koeberl, C., 2015. Microbially mediated deposition of postglacial transition layers from the Neoproterozoic Otavi Group, Namibia: evidence of rapid deglaciation after the Sturtian Cryogenic period. *Carpathian Journal of Earth and Environmental Sciences*, 10, 63-76.
- Harland, W.B., 1964. Critical evidence for a great Infra-Cambrian glaciation. *Geologische Rundschau*, 54, 45-61.
- Hedberg, R.M., 1979. Stratigraphy of the Owamboland basin, South West Africa. *Bulletin of Precambrian Research Unit*, 1979, Cape Town, 24, 325 pp.
- Heim, C.N., 2010. An integrated approach to the study of bio-signatures in mineralizing biofilms and microbial mats. PhD thesis, Georg-August-University of Gottingen, Germany. 183 pp.
- Herdianita, N.R., Browne, P.R.L., Rodgers, K.A. and Campbell, K.A., 2000. Mineralogical and textural changes accompanying ageing of silica sinter. *Mineralium Deposita*, 35, 48-62.
- Hoffman, P.F. and Halverson, G.P., 2008. Otavi Goup of the western Northern Platform, the Eastern Kaoko Zone and the western Northern Margin Zone.- In: R. McG. Miller (Ed): *The Geology of Namibia - Vol 2: Neoproterozoic to Lower Paleozoic*. Ministry of Mines and Energy, Geological Survey, Namibia 69-136.
- Hoffman, P.F. and Schrag, D.P., 2000. Snowball Earth. *Scientific American*, 282,1, 50-57.
- Hoffman, P.F. and Schrag, D.P., 2002. The snowball Earth hy-

- pothesis: testing the limits of global change. *Terra Nova*, 14, 129-155. <http://dx.doi.org/10.1046/j.1365-3121.2002.00408.x>
- Hoffman, P.F., 2002. Carbonates bounding glacial deposits: Evidence for Snowball Earth episodes and greenhouse aftermaths in the Neoproterozoic Otavi Group of northern Namibia. *Excursion Guide, 16th International Sedimentological Conference, Auckland Park, South Africa*, 39 p.
- Hoffman, P.F., Kaufman, A.J., Halverson, G.P. and Schrag, D.P., 1998a. A Neoproterozoic Snowball Earth. *Science*, 281, 1342–1346.
- Hoffman, P.F., Kaufman, J.A. and Halverson, G.P., 1998b. Comings and goings of global glaciations on a Neoproterozoic carbonate platform in Namibia. *GSA Today*, 8, 1-9.
- Hoffman, P.F., MacDonald, F.A. and Halverson, G.P., 2011. Chemical sediments associated with Neoproterozoic glaciation: iron formation, cap carbonate, barite and phosphorite. In: Arnaud E., Halverson G.P., Shields-Zhou G. (Eds.): *The Geological Record of Neoproterozoic Glaciations*. Geological Society of London, Memoir, 36, 67-80. <http://dx.doi.org/10.1144/M36.5>
- Hoffmann, K.-H. and Prave, A.R., 1996. A preliminary note on a revised subdivision and regional correlation of the Otavi Group based on glaciogenic diamictites and associated cap dolostones. *Communications of the Geological Society of Namibia*, 11, 81-86.
- Kennedy, M. J., Mrofka, D. and von der Borch, C., 2008. Snowball Earth termination by destabilization of equatorial permafrost methane clathrate. *Nature*, 453, 642-645. <http://dx.doi.org/10.1038/nature06961>
- Kennedy, M.J., Christie-Blick, N. and Sohl, L.E., 2001. Are Proterozoic cap carbonates and isotopic excursions a record of gas hydrate destabilization following Earth's coldest intervals? *Geology*, 29, 443-446.
- Konhauser, K., O. (Ed.) 2012. *Fundamentals of Geobiology*, Wiley - Blackwell Science Ltd, New York. 210 pp.
- Konhauser, K.O., 1998. Diversity of bacterial iron mineralization. *Earth-Science Reviews*, 43, 91-121.
- Konhauser, K.O., Hamade, T., Raiswell, R., Morris, R.C., Ferris, F. G., Southam, G. and Canfield, D.E., 2002. Could bacteria have formed the Precambrian banded iron formations? *Geology*, 20, 1079-1082.
- Le Ber, E., Le Heron, D. P. G., Winterleitner, D. W. J. Bosence, Vining, B. A. and Kamona, F., 2013. Microbialite recovery in the aftermath of the Sturtian glaciation: Insights from the Rasthof Formation, Namibia. *Sedimentary Geology*, 294, 1-12. <https://doi.org/10.1016/j.sedgeo.2013.05.003>
- Le Heron, D., Busfield, M., Le Ber, E. and Kamona, A., 2013. Neoproterozoic ironstones in northern Namibia: Biogenic precipitation and Cryogenian glaciation. *Palaeogeography, Palaeoclimatology, Palaeoecology*, 369, 48-57. <https://doi.org/10.1016/j.palaeo.2012.09.026>
- Le Hir, G., Donnadieu, Y., Godderis, Y., Pierrehumbert, R.T., Halverson, G.P., Macouin, M., Nedelec, A. and Ramstein, G., 2008. The snowball Earth aftermath: Exploring the limits of continental weathering processes. *Earth and Planetary Science Letters*, 277, 453-463. <https://doi.org/10.1016/j.epsl.2008.11.010>
- Maruoka, T., Koeberl, C. and Bohor, B.F., 2007. Carbon isotopic compositions of organic matter across continental Cretaceous–Tertiary (K–T) boundary sections: Implications for paleo-environment after the K–T impact event. *Earth Planetary Science Letters*, 253, 226–238. <https://doi.org/10.1016/j.epsl.2006.10.028>
- Maruoka, T., Koeberl, C., Matsuda, J. and Syono, Y., 2003. Carbon isotope fractionation between graphite and diamond during shock experiments. *Meteoritics and Planetary Science*, 38, 1255–1262. <http://dx.doi.org/10.1111/j.1945-5100.2003.tb00311.x>
- Mettreux, M., Homewood, P., Dos Anjos, C., Erthal, M., Lima, R., Matsuda, N., Souza, A. and Al Balushi, S., 2015. Microbial communities and their primary to early diagenetic mineral phases; the record from Neoproterozoic microbialites of Qarn Alam, Oman. *Geological Society, London, Special Publications*, 418. <http://dx.doi.org/10.1144/SP418.5>
- Meyer, E. E., Quicksall, A.N., Landis, J.D., Link, P.K. and Bostick, B.C., 2012. Trace and rare earth elemental investigation of a Sturtian cap carbonate, Pocatello, Idaho: Evidence for ocean redox conditions before and during carbonate deposition. *Precambrian Research*, 192-195, 89–106. <http://dx.doi.org/10.1016/j.precamres.2011.09.015>
- Mickala, O.R., Fournier, F., Affaton, P., Vidal, L., Mounguengui, M. M., Boudzoumou, F., Nganga, D.M.M., Vandamme, D., Miche, N. and Borschneck, D., 2015. Microfacies, paleoenvironments and development pattern of Neoproterozoic Cap Carbonates in the Niari-Nyanga Basin (Congo and Gabon Republics, Central Africa). *Journal of African Earth Sciences*, 109, 27-36. <https://doi.org/10.1016/j.jafrearsci.2015.05.009>
- Molnár Zs, Polgári M, Hein J.R., Józsa S., Fekete J., Gyollai I., Fintor K., Bíró L., Szabó M., Rapi S., Forgó P., Vigh T. (2017) Fe-Mn oxide indications in the feeder and mound zone of the Jurassic Mn-carbonate ore deposit, Úrkút, Hungary. *Ore Geology Reviews*, 86, 839-855. DOI:10.1016/j.oregeorev.2016.11.005
- Polgári, M., Hein, J. R., Tóth, A. L., Pál-Molnár, E., Vigh, T., Bíró, L. and Fintor, K., 2012b. Microbial action formed Jurassic Mn-carbonate ore deposit in only a few hundred years (Úrkút, Hungary). *Geology*, 40/10, 903–906. 10.1130/G33304.1
- Polgári, M., Hein, J.R., Vigh, T., Szabó-Drubina, M., Fórizs, I., Bíró, L., Müller, A. and Tóth, A.L., 2012a. Microbial processes and the origin of the Úrkút manganese deposit, Hungary. *Ore Geology Reviews*, 47, 87–109. <https://doi.org/10.1016/j.oregeorev.2011.10.001>
- Preat, A., Mamet, B., De Ridder, C., Boulvain, F. and Gillan, D., 2000. Iron bacterial and fungal mats, Bajocian stratotype (Mid-Jurassic, northern Normandy, France). *Sedimentary Geology*, 137, 107–126.
- Pruss, S.B., Bosak, T., McDonald, F. A., McLane, M. and Hoffman, P.F., 2010. Microbial facies in a Sturtian cap carbonate, the Rasthof Formation, Otavi Group, northern Namibia. *Precambrian Research*, 181, 187–198. <https://doi.org/10.1016/j.precamres.2010.06.006>

- Rajabzadeh, M.A., Haddad, F., Polgári, M., Fintor, K., Walter, H., Molnár, Zs. and Gyollai, I., 2017. Investigation on the role of microorganisms in manganese mineralization from Abadeh-Tashk area, Fars Province, southwestern Iran by using petrographic and geochemical data. *Ore Geology Reviews*, 80, 229-249. <https://doi.org/10.1016/j.oregeorev.2016.06.035>
- Reysenbach, A. and Cady, S., 2001. Microbiology of ancient and modern hydrothermal systems. *Trends of Microbiology*, 9, 79–86.
- Rimmer, S., 2004. Geochemical paleoredox indicators in Devonian-Mississippian black shales, Central Appalachian Basin (USA). *Chemical Geology*, 206, 373–391. <https://doi.org/10.1016/j.chemgeo.2003.12.029>
- Rooney, A.D., Strauss, J.V., Brandon, A.D. and Macdonald, F.A., 2015. A Cryogenian chronology: Two long-lasting synchronous Neoproterozoic glaciations. *Geology*, 43/5, 459-462. <http://dx.doi.org/10.1130/G36511.1>
- SACS, 1980. South Africa Committee for Stratigraphy 1980. *Stratigraphy of South Africa*. Kent L.E. (Comp); Part 1. Lithostratigraphy of the Republic of South Africa, South West Africa / Namibia and the Republics of Bophuthatswana, Transkei and Venda. Handbook Geological Survey of South Africa, 8, 690 pp.
- Schwertmann, U. and Cornell, R.M., 2007. *Iron Oxides in the Laboratory: Preparation and Characterization*. Wiley-VCH, 188 pp.
- Stanistreet, I.G., Kukla, P.A. and Henry, G., 1991. Sedimentary basinal response to a Late Precambrian Wilson Cycle: The Damara Orogen and Nama Foreland, Namibia. *Journal of African Earth Sciences*, 13, 41-156. [https://doi.org/10.1016/0899-5362\(91\)90048-4](https://doi.org/10.1016/0899-5362(91)90048-4)
- Takahashi, Y., Hirata, T., Shimizu, H., Ozaki, T. and Fortin, D., 2007. A rare earth element signature of bacteria in natural waters? *Chemical Geology*, 244/3–4, 569-583. <https://doi.org/10.1016/j.chemgeo.2007.07.005>
- van Smeerdjik Hood, A. and Wallace, M.W., 2015. Extreme ocean anoxia during the Late Cryogenian recorded in reefal carbonates of Southern Australia. *Precambrian Research*, 261, 96-111. <https://doi.org/10.1016/j.precamres.2015.02.008>
- Verkouteren, R.M. and Klinedinst, D.B., 2004. Value Assignment and Uncertainty Estimation of Selected Light Stable Isotope Reference Materials. NIST Special Publication, 260, p.149.
- Wen, B., Evans, D.A., Li, Y.X., Wang, Z. and Liu, C., 2015. Newly discovered Neoproterozoic diamictite and cap carbonate (DCC) couplet in Tarim Craton, NW China: Stratigraphy, geochemistry, and paleoenvironment. *Precambrian Research*, 271, 278-294. <https://doi.org/10.1016/j.precamres.2015.10.006>
- Williams, G.E., 2000. Geological constraints on the Precambrian history of Earth's rotation and the Moon's orbit. *Reviews of Geophysics*, 38, 37-59.
- Williams, G.E., Schmidt, P.W. and Embleton, B.J.J., 1995. Comment on 'The Neoproterozoic (1000-540 Ma) glacial intervals: No more snowball Earth?' by Joseph G. Meert and Rob van der Voo. *Earth and Planetary Science Letters*, 131, 115-122.
- Yang, B., Hu, B., Bao, Z., Zhang, Z., 2011. REE geochemical characteristics and depositional environment of the black shale-hosted Baiguoyuan Ag-V deposit in Xingshan, Hubei Province, China. *Journal of Rare Earths*, 29, 499–506. [https://doi.org/10.1016/S1002-0721\(10\)60488-7](https://doi.org/10.1016/S1002-0721(10)60488-7)

Received: 19 April 2016

Accepted: 10 April 2017

Ildikó GYOLLAJ¹⁾²⁾, Márta POLGÁRI²⁾³⁾, Krisztián FINTOR⁴⁾, Elemér PÁL-MOLNÁR⁴⁾, Friedrich POPP⁵⁾ & Christian KOEBERL¹⁾⁶⁾

¹⁾ Department of Lithospheric Research, University of Vienna, Althanstrasse 14, A-1090 Vienna, Austria;

²⁾ Research Center for Astronomy and Geosciences, Geobiomineralization and Astrobiological Research Group, Institute for Geology and Geochemistry, Hungarian Academy of Sciences, 1112 Budapest, Budaörsi str. 45, Hungary;

³⁾ Eszterházy Károly University, Dept. of Physical Geography and Geoinformatics, Leányka str. 6, 3300 Eger, Hungary;

⁴⁾ Szeged University, Department of Mineralogy, Geochemistry and Petrology, Egyetem str. 2-6, 6702 Szeged, Hungary;

⁵⁾ Department of Geodynamics and Sedimentology, University of Vienna, Althanstrasse 14, A-1090 Vienna, Austria;

⁶⁾ Natural History Museum, Vienna, A-1010 Burgring 7, Vienna, Austria;

^{*)} Corresponding author, rodokrozzit@gmail.com